Self-organisation and non-linear dynamics in driven magnetohydrodynamic turbulent flows

V. Dallas and A. Alexakis

Citation: Physics of Fluids (1994-present) **27**, 045105 (2015); doi: 10.1063/1.4916971
View online: http://dx.doi.org/10.1063/1.4916971
View Table of Contents: http://scitation.aip.org/content/aip/journal/pof2/27/4?ver=pdfcov
Published by the AIP Publishing

PHYSICS OF FLUIDS **27**, 045105 (2015)

Self-organisation and non-linear dynamics in driven magnetohydrodynamic turbulent flows

V. Dallas and A. Alexakis
Laboratoire de Physique Statistique, École Normale Supérieure, CNRS, Université Pierre et Marié Curie, Université Paris Diderot, 24 rue Lhomond, 75005 Paris, France

(Received 20 November 2014; accepted 25 March 2015; published online 13 April 2015)

Magnetohydrodynamic (MHD) turbulent flows driven by random, large-scale, mechanical and electromagnetic external forces of zero helicities are investigated by means of direct numerical simulations. It is shown that despite the absence of helicities in the forcing, the system is attracted to helical states of large scale condensates that exhibit laminar behaviour despite the large value of the Reynolds numbers examined. We demonstrate that the correlation time of the external forces controls the time spent on these states, i.e., for short correlation times, the system remains in the turbulent state while as the correlation time is increased, the system spends more and more time in the helical states. As a result, time averaged statistics are significantly affected by the time spent on these states. These results have important implications for MHD and turbulence theory and they provide insight into various physical phenomena where condensates transpire. © *2015 AIP Publishing LLC*. [http://dx.doi.org/10.1063/1.4916971]

I. INTRODUCTION

The formation of large scale condensates from homogeneous turbulence has been observed in various flows such as in 2D turbulent flows,[1] flows under the effect of rotation,[2] or the combined effect of rotation and stratification.[3–5] In magnetohydrodynamic (MHD) theory, relaxation processes have been recognised to explain the evolution of electrically conducting fluids towards special states of self-organisation, where large scale condensates emerge as a consequence of multiple conservation laws.[6] For homogeneous, incompressible, ideal MHD with zero mean magnetic field, there are three known quadratic conserved quantities: the total energy $E \equiv E_u + E_b = \frac{1}{2}\langle |\boldsymbol{u}|^2 + |\boldsymbol{b}|^2 \rangle_V$, the magnetic helicity $H_b \equiv \langle \boldsymbol{a} \cdot \boldsymbol{b} \rangle_V$, and the cross-helicity $H_c \equiv \langle \boldsymbol{u} \cdot \boldsymbol{b} \rangle_V$. Here, $\boldsymbol{u}$ is the velocity field, $\boldsymbol{b} \equiv \boldsymbol{\nabla} \times \boldsymbol{a}$ is the magnetic field, where $\boldsymbol{a}$ is the solenoidal magnetic potential, and $\langle \cdot \rangle_V$ stands for spacial averages over the volume V.

The dissipative relaxation processes in decaying MHD turbulence are the Taylor relaxation[7–9] and the dynamic alignment.[10,11] These states could be derived analytically by minimising an energy integral subject to some constraints.[12] In detail, Taylor relaxation is associated with the decay of turbulence towards a minimum energy state under the constraint of finite H_b. The solution to this variational problem is a *force-free* field, where $\boldsymbol{u} = 0$ and $\boldsymbol{\nabla} \times \boldsymbol{b} = \lambda' \boldsymbol{b}$ with the Lagrange multiplier $\lambda' \equiv \int \boldsymbol{b}_{min}^2 \, dV / H_b$. On the other hand, the slow decay of H_c in comparison to E can lead to a minimum energy state while cross-helicity is conserved, where self-organisation occurs due to dynamic alignment between the velocity and the magnetic field, i.e., $\boldsymbol{u} = \pm \boldsymbol{b}$. This relaxed state is called *Alfvénic state*. These relaxation processes can be seen as a *selective decay*[13] between the conserved quantities due to their very different rates of dissipation in turbulent flows, and they have also been shown to operate locally in space quenching the non-linearities.[14]

The relaxation to the force-free state was offered as an explanation in reversed-field pinch plasma devices[9,15] and it has also been used to estimate the energy release in coronal structures in connection to the problem of coronal heating.[16,17] Moreover, the Alfvénic states have been frequently observed in solar wind turbulence.[18,19] The growth of correlation between $\boldsymbol{u}$ and $\boldsymbol{b}$ in solar wind was conjectured to emerge dynamically from MHD turbulence[20] and this was verified in

direct numerical simulations (DNSs) of undriven turbulent flows.[21] More recently, such correlation was observed using *in situ* measurements of fast, high latitude solar wind data taken by spacecrafts.[22,23] Moreover, Stribling and Matthaeus[24] have shown numerically that in a truncated model of three-dimensional decaying MHD turbulence, the final states depend on the initial values of H_b and H_c. In particular, they showed that the final state for strongly helical initial conditions is the force-free field, whereas for sufficient large initial alignment between $\boldsymbol{u}$ and $\boldsymbol{b}$ is the Alfvénic state.

In this paper, we show that large scale helical condensates due to force-free, Alfvénic, and Beltrami (i.e., $\boldsymbol{\nabla}\times\boldsymbol{u}\propto\boldsymbol{u}$) states can occur in driven MHD turbulent flows from initial conditions and external forces of zero helicity. Large scale condensates manifest themselves when a developing inverse cascade meets the largest scale of the system (box-size). In their presence, long-time variations of the amplitude of fluctuations are observed with a frequency spectrum of the form $1/f$ (where f is the frequency). Such $1/f$ spectra have been observed in decaying and forced MHD[25–27] and in dynamo reversals.[28] Our work moves in the opposite direction and investigates the effect of long time correlation of the forcing on the formation of such condensates. We demonstrate that these states appear when the correlation time scale of the external forces is sufficiently large. Our results thus bring up important implications on the way MHD turbulent flows should be forced in numerical simulations. Moreover, this work may provide insight into self-organisation processes and the dynamics of helicity in fluid and plasma flows.

The paper is structured as follows. All the necessary details on our DNS of driven MHD turbulent flows are provided in Sec. II. Section III analyses the non-linear dynamics of the helical states. In particular, we focus on the dependence of the MHD flows on the forcing correlation time scale, its effect on the growth of helicities, and the fate of the magnetic helical condensates. Individual statistics of the velocity and the magnetic field are presented in Sec. IV, where different dynamics are obeyed at different instances. Finally, in Sec. V, we conclude by summarising our findings and we discuss the implications of our work.

II. NUMERICAL METHODS

Our study is based on numerical simulations of the MHD equations

$$(\partial_t-\nu\boldsymbol{\Delta})\boldsymbol{u}=(\boldsymbol{u}\times\boldsymbol{\omega})+(\boldsymbol{j}\times\boldsymbol{b})-\boldsymbol{\nabla}P+\boldsymbol{f}_u, \tag{1}$$

$$(\partial_t-\mu\boldsymbol{\Delta})\boldsymbol{b}=\boldsymbol{\nabla}\times(\boldsymbol{u}\times\boldsymbol{b})+\boldsymbol{f}_b, \tag{2}$$

where the vorticity $\boldsymbol{\omega}\equiv\boldsymbol{\nabla}\times\boldsymbol{u}$, the current density $\boldsymbol{j}\equiv\boldsymbol{\nabla}\times\boldsymbol{b}$, P is the pressure, ν is the kinematic viscosity, μ is the magnetic diffusivity, $\boldsymbol{f}_u$ is the mechanical external force, and $\boldsymbol{f}_b$ is the electromagnetic external force. Using the pseudo-spectral method, we numerically solve Eqs. (1) and (2) in a three-dimensional periodic box of size 2π, satisfying $\boldsymbol{\nabla}\cdot\boldsymbol{u}=\boldsymbol{\nabla}\cdot\boldsymbol{b}=0$. Aliasing errors are removed using the 2/3 dealiasing rule, i.e., wavenumbers $k_{min}=1$ and $k_{max}=N/3$, where N is the number of grid points in each Cartesian coordinate. For more details on the numerical code, see Refs. 29 and 30.

In our simulations, the velocity and the magnetic field are forced randomly as follows:

$$\boldsymbol{f}_u=f_0\sum_{k_f}\begin{pmatrix}\sin(k_fz+\phi_z)+\sin(k_fy+\phi_y)\\ \sin(k_fx+\phi_x)+\sin(k_fz+\phi_z)\\ \sin(k_fy+\phi_y)+\sin(k_fx+\phi_x)\end{pmatrix}, \tag{3}$$

$$\boldsymbol{f}_b=f_0\sum_{k_f}\begin{pmatrix}-\sin(k_fz+\phi_z)+\sin(k_fy+\phi_y)\\ -\sin(k_fx+\phi_x)+\sin(k_fz+\phi_z)\\ -\sin(k_fy+\phi_y)+\sin(k_fx+\phi_x)\end{pmatrix}, \tag{4}$$

where their amplitudes are normalised such that $|\boldsymbol{f}_u|=|\boldsymbol{f}_b|=f_0=1$ for all runs. The phases ϕ_x, and ϕ_y, ϕ_z are randomly chosen for $k_f=1$ and 2 every τ_c, which we call the forcing correlation time scale. τ_c was chosen to take values from $0.5\tau_f$ to $8\tau_f$, where $\tau_f\equiv(k_{min}f_0)^{-1/2}$. Moreover, we consider runs with $\tau_c/\tau_f=\infty$ indicating constant phases in time. In other words, we randomise the phases only once, at $t=0$, in the duration of the runs. Note that the forces have zero helicities,

TABLE I. Numerical parameters of the DNS. Note that the empty spaces in the table correspond to the runs that were not able to reach a steady state.

τ_c/τ_f	N	k_f	$\nu = \mu$	Re_L	Re_λ	L	λ	u'	b'
0.5	64	1-2	1×10^{-1}	18.5	13.5	1.81	1.32	1.02	1.24
0.5	64	1-2	5×10^{-2}	37.6	23.9	1.65	1.05	1.14	1.39
0.5	64	1-2	2×10^{-2}	90.6	46.3	1.45	0.74	1.25	1.55
0.5	64	1-2	1×10^{-2}	174.2	72.1	1.33	0.55	1.31	1.65
8.0	64	1-2	1×10^{-1}	25.1	17.5	1.77	1.23	1.42	1.81
8.0	64	1-2	5×10^{-2}	52.2	34.0	1.75	1.14	1.49	2.62
8.0	64	1-2	2×10^{-2}	255.1	187.2	2.18	1.60	2.34	6.72
∞	64	1-2	1×10^{-2}	526.7	472.0	2.31	2.07	2.28	31.74
0.5	128	1-2	5×10^{-3}	340.2	110.7	1.26	0.41	1.35	1.78
1.0	128	1-2	5×10^{-3}	377.7	122.1	1.33	0.43	1.42	2.05
2.0	128	1-2	5×10^{-3}	685.1	307.9	1.98	0.89	1.73	4.78
4.0	128	1-2	5×10^{-3}	1210.0	731.5	2.20	1.33	2.75	8.57
8.0	128	1-2	1×10^{-2}	830.3	608.9	2.25	1.65	3.69	9.64
8.0	128	1-2	5×10^{-3}	1680.0	1132.5	2.24	1.51	3.75	11.91
∞	128	1-2	5×10^{-3}	...	...	...	...	...	...
0.5	256	1-2	2×10^{-3}	798.0	189.0	1.14	0.27	1.40	1.79
∞	256	1-2	2×10^{-3}	...	...	...	...	...	...
∞	256	2-4	2.5×10^{-3}	...	...	...	...	...	...
∞	256	4-8	1.5×10^{-3}	...	...	...	...	...	...
0.5	512	1-2	1×10^{-3}	1591.4	277.4	1.09	0.19	1.46	1.91
∞	512	1-2	9×10^{-4}	...	...	...	...	...	...

i.e., $\langle \boldsymbol{f}_{u,b} \cdot \boldsymbol{\nabla} \times \boldsymbol{f}_{u,b} \rangle_V = \langle \boldsymbol{f}_u \cdot \boldsymbol{f}_b \rangle_V = 0$. The energies of the initial conditions are chosen to be in equipartition (viz., $E_u = E_b = 0.5$) unlike in studies of relaxation processes,[24,31] where the initial conditions were chosen to have a tendency towards a particular relaxation state (i.e., force-free or Alfvénic). The magnetic Prandtl number is unity (i.e., $\nu = \mu$) for all the runs. All the necessary parameters of our DNS are presented in Table I. Only for those runs that reached a steady state, we also tabulate the rms values of the velocity u' and the magnetic field b', the integral length scale $L \equiv \frac{3\pi}{4} \int k^{-1} E(k) dk / \int E(k) dk$, the Taylor micro-scale $\lambda \equiv (5 \int E(k) dk / \int k^2 E(k) dk)^{1/2}$, and the Reynolds numbers $Re_L = u' L/\nu$ and $Re_\lambda = u' \lambda / \nu$.

III. FORCE-FREE, ALFVÉNIC, AND BELTRAMI ASYMPTOTIC STATES

To start with, we consider the temporal evolution of our flows with different forcing correlation time scales. Remarkably, as τ_c/τ_f increases, we observe the amplitude of all space averaged quadratic quantities to increase substantially. This is depicted indicatively by the time-series of the total energy in Fig. 1 plotted on a logarithmic scale. The inset shows the mean value of total energy $\langle E \rangle_t$ with respect to τ_c/τ_f. Here, the angle brackets $\langle \cdot \rangle_t$ denote temporal averages. As the forcing correlation time scale increases from $\tau_c/\tau_f = 0.5$ to 8, the mean value of total energy $\langle E \rangle_t$ increases by almost two orders of magnitude and strongly fluctuates varying by an order of magnitude. Note that the time-series is characterised by dynamical time scales much greater than τ_c, τ_f, and the non-linear time scale $\tau_{NL} \equiv 1/(k_{min} \langle |\boldsymbol{u}|^2 \rangle_V^{1/2})$. This behaviour is caused by the creation of large scale condensates in our flows, which will become more obvious later on in our analysis. Due to these long dynamical time scales and the large variations, we are compelled to integrate very far in time to obtain converged statistics and consequently deal with moderate resolutions.

In Fig. 2, we present the Probability Density Functions (PDFs) of the time series of the normalised cross, magnetic, and kinetic helicities,

$$\rho_c \equiv H_c / (\langle |\boldsymbol{u}|^2 \rangle_V^{1/2} \langle |\boldsymbol{b}|^2 \rangle_V^{1/2}), \tag{5}$$

$$\rho_b \equiv k_{min} H_b / \langle |\boldsymbol{b}|^2 \rangle_V^{1/2}, \tag{6}$$

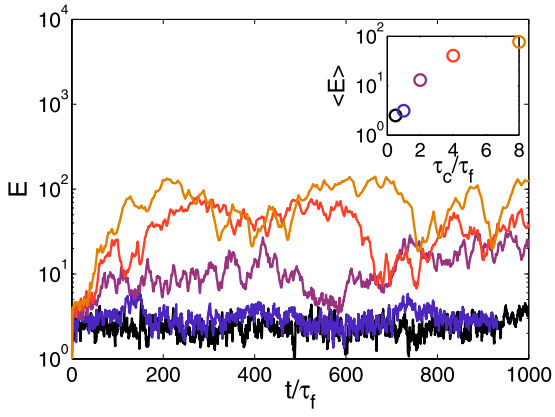

FIG. 1. Time-series of total energy for the 128^3 runs with different forcing correlation time scales. The inset shows the value of the time average total energy with respect to τ_c/τ_f.

$$\rho_u \equiv H_u/(\langle|\boldsymbol{u}|^2\rangle_V^{1/2}\langle|\boldsymbol{\omega}|^2\rangle_V^{1/2}), \tag{7}$$

respectively. For low values of τ_c/τ_f, the PDFs of the normalised helicities are peaked around 0 as it is expected (see Fig. 2). However, for higher values of τ_c/τ_f, the PDFs become broader and shallower. For $\tau_c/\tau_f \geq 4$, the PDF of magnetic helicity in Fig. 2(a) peaks at 1 indicating the reach of a force-free state $\boldsymbol{j} \propto \boldsymbol{b}$ and thus, $\boldsymbol{j} \times \boldsymbol{b} = 0$. The PDF of the normalised cross-helicity in Fig. 2(b) also peaks at 1 for $\tau_c/\tau_f = 8$ indicating full Alfvénisation of the flow (i.e., $\boldsymbol{u} = \pm\boldsymbol{b}$). In the case of the normalised kinetic helicity, the PDFs with low τ_c/τ_f values are peaked at 0 and they increase significantly for higher τ_c/τ_f values without reaching full Beltramisation (i.e., $|\rho_u| = 1$ or $\boldsymbol{u} \propto \boldsymbol{\omega}$) even for $\tau_c/\tau_f = 8$ (see Fig. 2(c)). The preference to these highly helical states, where non-linearities (and the cascade to small scales) are quenched, is related to the excess of energy that was observed in Fig. 1.

Now we examine the evolution of our flows in a three-dimensional phase space composed by the three normalised helicities. Figure 3 demonstrates the time evolution of the solutions of our flows and their dependence on the forcing correlation time τ_c/τ_f, which varies from 0.5 to ∞. In particular, Fig. 3(a) shows the phase sub-space of the normalised magnetic and cross helicities, where we observe that the flows with $\tau_c/\tau_f = 0.5$ and 1 mainly oscillate around the 0 origin with some excursions away from 0. As the forcing correlation time scale increases from $\tau_c/\tau_f = 2$ to ∞, we notice that these excursions are trapped into two attracting solutions $\rho_b \simeq \pm 1$, oscillating between $-1 \leq \rho_c \leq 1$ for long times. In other words, the runs with long forcing correlation times are trapped into force-free states (i.e., $\boldsymbol{j} \propto \boldsymbol{b}$) without observing noise driven escape from one basin of attraction to the other. On the other hand, the system undergoes noise driven escape between the two attracting solutions of the Alfvénic states (i.e., $\boldsymbol{u} = \pm\boldsymbol{b}$). It is of interest to mention here that the choice between the two asymptotic fully magnetically helical states depends sensitively on

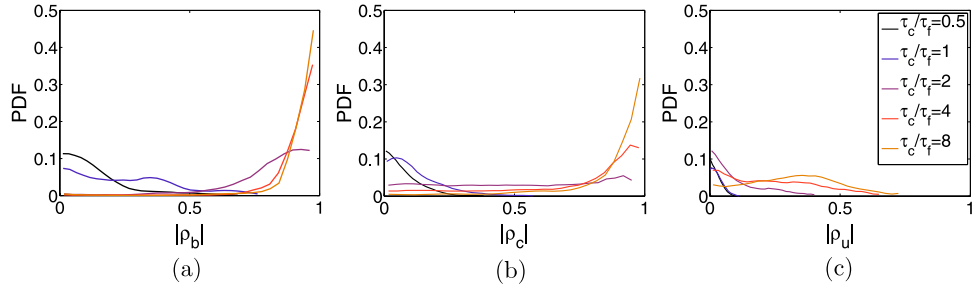

FIG. 2. Probability Density Functions of the absolute value of the normalised (a) magnetic helicity $|\rho_b|$, (b) cross-helicity $|\rho_c|$, and (c) kinetic helicity $|\rho_u|$ for the 128^3 runs with different τ_c/τ_f.

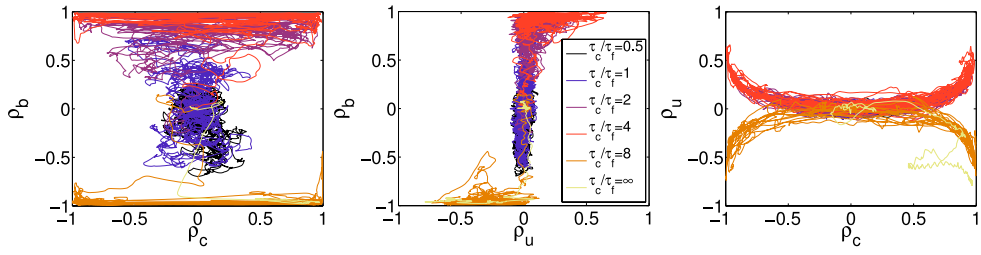

FIG. 3. Phase sub-space of (a) ρ_b and ρ_c, (b) ρ_b and ρ_u, (c) ρ_u and ρ_c for the 128^3 runs with different τ_c/τ_f.

the initial conditions. A small perturbation in magnetic helicity can lead the system to be trapped either in the $\rho_b = 1$ or -1 state, much like a small variation in the initial conditions of a coin-toss experiment can alter the final results from head to tails.[32]

The phase sub-space of the normalised magnetic and kinetic helicity (see Fig. 3(b)) reveals two states with positive and negative H_u for high enough values of τ_c/τ_f. Note that kinetic helicity grows only when $|\rho_b| > 0.5$ and always has the same sign with magnetic helicity. This implies that as the magnetic field becomes strong enough, it forces the flow to become Alfvénized (i.e., $\boldsymbol{u} \propto \boldsymbol{b}$) fluctuating between positive and negative H_c but always keeping the same sign for H_u and H_b (see Fig. 3) because kinetic and magnetic helicities are invariant under $\boldsymbol{u} \to -\boldsymbol{u}$ and $\boldsymbol{b} \to -\boldsymbol{b}$ transformations, respectively. For completeness of the three-dimensional phase space of normalised helicities, the phase sub-space of kinetic and cross-helicity is presented in Fig. 3(c). Here, the two attractors of positive and negative H_u are also evident, with the flows of high forcing correlation time scales to oscillate for long times between the $\boldsymbol{u} = \pm\boldsymbol{b}$ solutions, whereas the flows with low τ_c/τ_f to oscillate around $\rho_u = 0$.

The visualisations of vorticity contours in Fig. 4 clearly substantiate our results. Although forcing amplitudes, viscosities, and length scales are of the same order between the two flows (see also Table I), there is a distinct difference. For low τ_c/τ_f, the flow behaves more like fully developed homogeneous turbulence (see Fig. 4(a)), whereas for high enough time-correlated external forces, the flow becomes helical, the non-linearities and the cascade to small scales are suppressed, the energy is pilled up at the largest scales, and large cyclonic condensates are formed (see Fig. 4(b)).

At this point, we attempt to identify the fate of these helical condensates for flows with high enough time-correlated forces, high enough Reynolds numbers (for the flow to be fully turbulent),

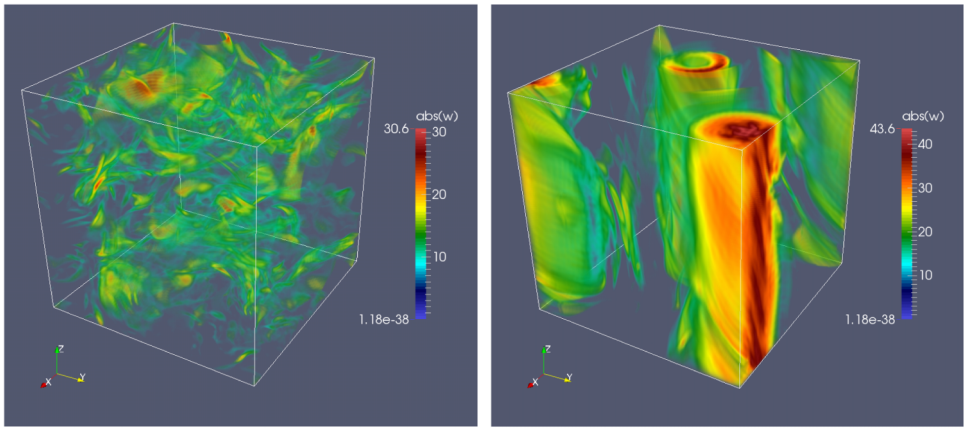

FIG. 4. Contours of the absolute value of vorticity for the 512^3 runs with (a) $\tau_c/\tau_f = 0.5$ and (b) $\tau_c/\tau_f = \infty$ (see also Table I).

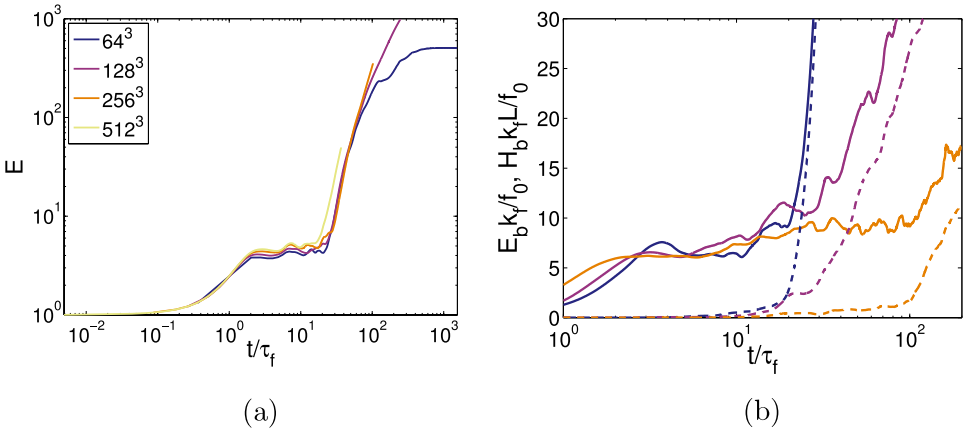

FIG. 5. (a) Time-series of the total energy for flows with different resolutions and fully time-correlated external forces, i.e. $\tau_c/\tau_f = \infty$. (b) Time-series of the magnetic energy (solid lines) and the absolute value of the magnetic helicity (dashed lines) for different forcing wavenumbers (i.e., blue (dark grey) lines k_f = 1-2, purple (grey) lines k_f = 2-4, orange (light grey) lines k_f = 4-8).

and $t \gg 1$. To illustrate this, we plot the time series of the total energy E for runs with $\tau_c/\tau_f = \infty$ at different resolutions (Fig. 5(a)). For early times, all the runs seem to asymptote towards a steady state solution (i.e., $t/\tau_f \simeq 10$). However, when we integrate further in time, the solutions deviate abruptly from this temporary steady state to higher levels of energy and helicities with the flows eventually to asymptote toward a laminar state at $t \gg 1$. Note that the reach of an asymptotic laminar state becomes prohibitive as resolution increases, because the time-step becomes vanishingly small, based on a Courant-Friedrichs-Lewy (CFL) criterion, in order to capture the required dynamics. On Fig. 5(b), the evolution of the magnetic energy is shown for flows forced at different length scales k_f. As the forcing wavenumber is increased and there is more scale separation between the box size and the forcing scale, the condensation is delayed but the general features are the same. At early times, a quasi-saturation occurs at amplitude $E_b \propto f_0/k_f$, with magnetic helicity small but gradually increasing. When the helicity becomes significantly strong ($H_b k_{min} \sim E_b$), the system transitions to the condensate state with a sharp increase of magnetic energy. The time scale for this transition increases with the scale separation. Thus, we expect the present results to persist at larger scale separations provided that the correlation time τ_c is long enough.

These laminar asymptotic solutions are clearly depicted in Fig. 6, where the dissipation coefficient $C_\epsilon \equiv \epsilon L/u'^3$ (with $\epsilon = \nu\langle|\boldsymbol{\omega}|^2\rangle + \mu\langle|\boldsymbol{j}|^2\rangle$, the total dissipation rate) is plotted for different Reynolds number flows. The triangles that represent runs with $\tau_c/\tau_f = 0.5$ seem to follow an asymptotic trend toward a finite value of dissipation independent of Re_L (i.e., $C_\epsilon \simeq const.$) and this

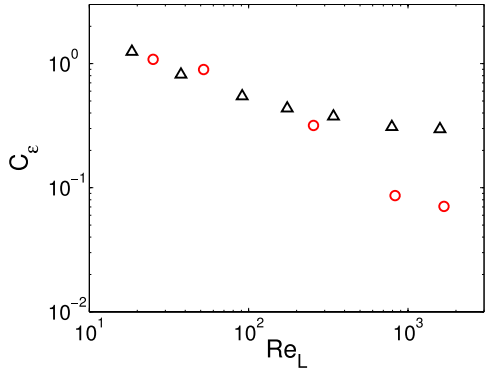

FIG. 6. Dissipation coefficient C_ϵ as a function of Reynolds number Re_L. The triangles indicate runs with $\tau_c/\tau_f = 0.5$ and the circles indicate runs with $\tau_c/\tau_f = 8$ (see Table I for details).

is expected for flows that are considered to be fully turbulent (see Fig. 4(a)). However, the circles that denote runs with $\tau_c/\tau_f = 8$ seem to be close to the laminar scaling $C_\epsilon \propto 1/Re_L$ with some small deviations due to the relatively moderate value of the forcing correlation time scale. The surprise here is that flows are attracted to the helical states that exhibit laminar behaviour even at such high Reynolds numbers (i.e., $Re_L \sim 2000$) where turbulence is usually expected to modify the laminar scaling.

Of course, the question that now arises is why these helical states manifest? These magnetic condensates can be shown to be unconditionally stable for any Reynolds number (see Subsection 1 of the Appendix) in contrast to Beltrami states in 3D helical hydrodynamic turbulence, which are unstable and energy is cascaded forward. So, this manifestation seems to be intimately connected with the presence of the electromagnetic force $\boldsymbol{f}_b$ that induces the condensation of E_b into a large scale helical magnetic field (magnetic condensates) and is a consequence of the unconditional stability of the helical condensates. We observe that condensation is induced in MHD turbulence as soon as an electromagnetic force $\boldsymbol{f}_b$ is involved in the equations, with either $|\boldsymbol{f}_b| \sim |\boldsymbol{f}_u|$ or $|\boldsymbol{f}_b| \gg |\boldsymbol{f}_u|$. Otherwise, when $\boldsymbol{f}_b = 0$ (i.e., dynamo) or $|\boldsymbol{f}_b| \ll |\boldsymbol{f}_u|$, helicities do not grow even for fully time-correlated forces, reaching a statistically steady state with helicities' fluctuations around zero. We further prove in Subsection 2 of the Appendix that in the extreme case when $\boldsymbol{f}_u = 0$ and the magnetic forcing is fully helical $\boldsymbol{f}_b = \lambda \boldsymbol{\nabla} \times \boldsymbol{f}_b$, the energy dissipation has a laminar scaling. Thus, no matter how large the Reynolds number is, the flow will not be effective in exciting small scales. Our simulations indicate that this also happens even when the forcing is not helical provided that τ_c/τ_f is large enough. In this case, the flow is attracted to one of the laminar stable helical states, despite the absence of helicity in the forcing, for any Reynolds number as Figs. 5 and 6 indicate. On the other hand, for small τ_c/τ_f, the external forces are modified before the system has time to reach a condensate state, and hence, a homogeneous turbulent flow is expected.

IV. STATISTICS OF HELICAL STATES

In contrast to the relaxation processes in selective decay, we are able to have statistics of the asymptotic force-free, Alfvénic, and Beltrami states. Figure 7 presents the magnetic and kinetic energy spectra averaged in time for the flows with different τ_c/τ_f. It is obvious that both the magnetic and kinetic energies increase significantly at low wavenumbers as τ_c/τ_f increases, suggesting the presence of condensates at large scales. Comparing the magnetic and the kinetic energy spectra, we observe that the magnetic helical condensates dominate the large scales of the flow with $\langle E_b \rangle_t > \langle E_u \rangle_t$ at low wavenumbers. As the external forces have longer correlation times, the ratio $\langle E_b \rangle_t / \langle E_u \rangle_t$ presents also a considerable increase at large scales. The slope of the energy spectrum appears to be very steep, particularly for high τ_c/τ_f values, and much steeper than

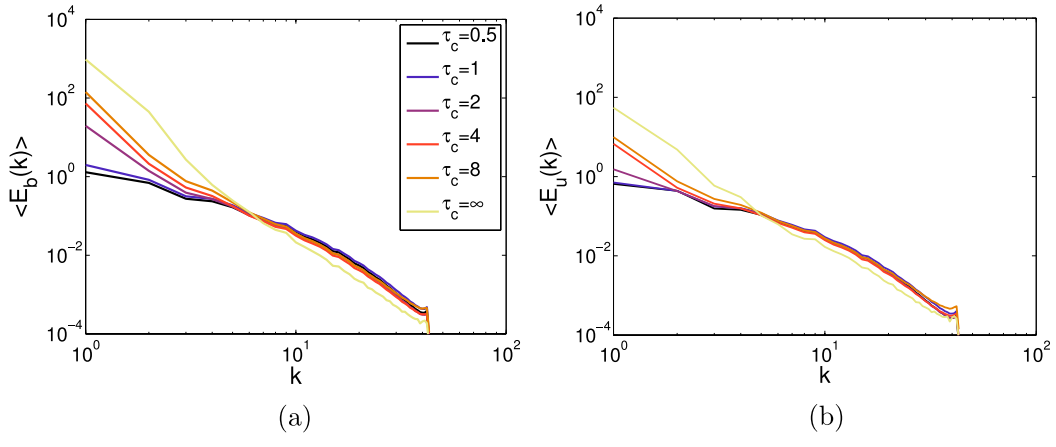

FIG. 7. Time averaged (a) magnetic and (b) kinetic energy spectra for the 128^3 runs with different values of τ_c/τ_f.

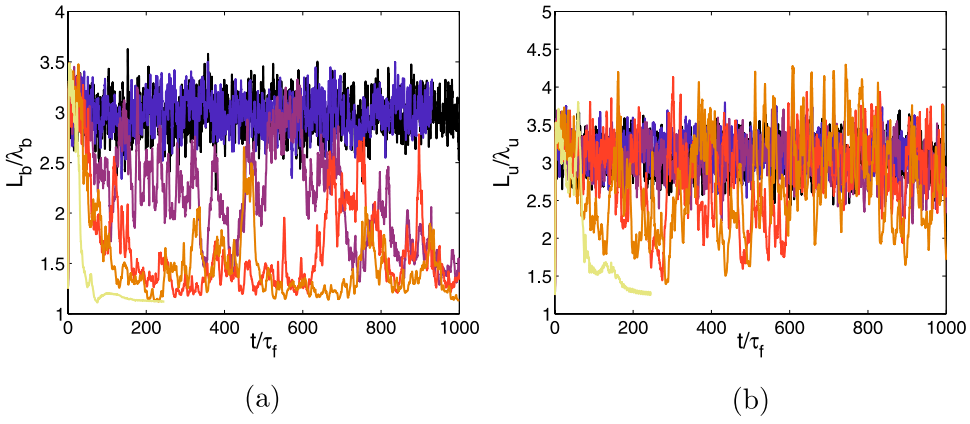

FIG. 8. Time-series of the ratio of the integral length scale to the Taylor micro-scale of (a) the magnetic field and (b) the velocity field for the 128^3 runs with forcing correlation time scales from $\tau_c/\tau_f = 0.5$ to ∞. Note that the curves follow the same labelling with Fig. 7.

typical turbulence theory exponents $-5/3$ and $-3/2$. Note that large fluctuations on the spectral exponent were observed throughout the run, with steep exponents during the condensate phases and more turbulent-like exponents within intermediate times. Therefore, the presence of the helicity condensates can clearly affect the time averaged energy spectrum even when their duration is short (e.g., for $\tau_c/\tau_f = 2$ in our flows).

Due to the relatively small resolution of these simulations, the statements about the spectral exponents are only qualitative. Alternatively, to show the existence of the large fluctuations that could affect the energy spectrum, we analyse the dynamics of the large and small scales. So, we compute the corresponding integral and Taylor length scales of the velocity and the magnetic field individually. In Fig. 8, we illustrate the time-series of the ratio of the integral length scale $L_{u,b}$ to Taylor micro-scale $\lambda_{u,b}$ of the magnetic field and the velocity field. When energy is concentrated on the largest scale of the system $k = 1$, the ratio $L_{u,b}/\lambda_{u,b} = \frac{3\pi}{4\sqrt{5}} \simeq 1.05$, and thus, the flow exhibits laminar behaviour. However, when $L_{u,b}/\lambda_{u,b} \gg 1$ a turbulent scaling is expected and dissipation is dominated by small scales. The difference in the dynamics of the velocity and the magnetic field is striking as the forcing correlation time scale varies. On one hand, the magnetic field reaches different asymptotic states for different values of τ_c/τ_f (see Fig. 8(a)) and it moves toward the laminar attractor, i.e., $L_b/\lambda_b \to 1$, as τ_c/τ_f becomes high enough. The time-series of L_b/λ_b is characterised by very rare and extreme events away from the condensate state laminar attractor for high values of τ_c/τ_f. On the other hand, even though the amplitude of the fluctuations of L_u/λ_u increases significantly with respect to the increase of the forcing correlation time scale, the mean value of L_u/λ_u remains almost at the same level except for the run with $\tau_c/\tau_f = \infty$ (see Fig. 8(b)). This diverse behaviour between the velocity and the magnetic field dominates the statistics and this was also depicted in the time-averaged energy spectra in Fig. 7. The large amplitude and rare fluctuations in the time-series of L_b/λ_b and L_u/λ_u imply that different spectra are obtained in different instances with this becoming more pronounced for the high values of the forcing correlation time scale. This behaviour seems to be valid for any Reynolds number flow with high enough time-correlated external forces.

V. DISCUSSION AND CONCLUSIONS

In this work, we consider MHD turbulent flows driven by kinetic and electromagnetic external forces. By increasing the time-correlation of the external forces τ_c, we demonstrate that MHD flows create large-scale condensates. This manifestation is connected with the presence of the electromagnetic external force (non-helical in this case), which induces the condensation of magnetic energy into the large scale helical coherent structures (i.e., condensates). The magnetic energy at the large

scales of the flow is always greater than the kinetic energy and the ratio of magnetic to kinetic energy grows as the forcing correlation time scale increases.

From our phase space analysis, we conclude that helicities increase as the forcing correlation time scale increases and drive the MHD flows toward condensate states at large integration times. Flows with high enough value of τ_c/τ_f reach different asymptotic states of different levels of helicities. The evolutions of these flows are governed by the force-free, Alfvénic, and Beltrami states (i.e., $\boldsymbol{u} \propto \boldsymbol{b} \propto \boldsymbol{\omega} \propto \boldsymbol{j}$), which appear to be attracting solutions of the MHD equations when $\tau_c/\tau_f \to \infty$ for any Reynolds number. The existence of these attractors is intimately connected to the unconditional stability of the magnetic helical condensates for any Reynolds number. So, a predictive theory in electromagnetically driven MHD turbulent flows is plausible based on the fact that asymptotic laminar attractors govern the dynamics of such flows with long enough forcing correlation time scales.

Moreover, the dynamics of the velocity and the magnetic field present very diverse dynamics, which dominate the statistics. At different instances in time, rare events provide very disparate energy spectra during the evolution of the MHD flows with high enough τ_c. These results raise the issue of how a DNS of MHD turbulent flows should be forced in order to avoid any misleading results to be caused by the large scale condensates of the flow. In particular, the current study excludes the use of time-independent electromagnetic forcing for the study of steady state MHD turbulence in periodic boxes as in this case, the flow will be attracted to the helical condensate states.

Our study has important implications for MHD and turbulence theory and perhaps provides insight into various physical phenomena where self-organisation manifests, such as in MHD and plasma experiments. The fact that helical states can persist for all times (if permitted by boundary conditions), leading to the suppression of the non-linearities and the system toward the laminar attractor, seems attractive. The presence of coherent structures inside turbulence greatly affects the plasma diffusion process. Therefore, further study of the self-organisation processes is vital in order to control the transport processes in fusion plasmas and hence, to improve the plasma confinement. Moreover, an increased knowledge of these phenomena in MHD turbulence can shed light on the understanding of some basic phenomena in solar corona, such as flares and coronal heating, which occur in a region where observations cannot be performed.

ACKNOWLEDGMENTS

The authors acknowledge interesting and useful discussions with Stephan Fauve. V.D. acknowledges the financial support from EU-funded Marie Curie Actions–Intra-European Fellowships (FP7-PEOPLE-2011-IEF, MHDTURB, Project No. 299973). The computations were performed using the HPC resources from GENCI-TGCC-CURIE (Project No. x2014056421).

APPENDIX: STABILITY AND BOUNDS

1. Unconditional stability of maximal helical states

Here, we show that magnetic helical condensates at the largest scale of MHD flows are unconditionally stable for any Reynolds number. We consider an arbitrary velocity field $\boldsymbol{u}'$ and a magnetic field with a large scale fully helical component $\boldsymbol{B}_0$ and a small scale component $\boldsymbol{b}'$, i.e., $\boldsymbol{b} = \boldsymbol{B}_0 + \boldsymbol{b}'$. The large scale magnetic field is such that

$$\boldsymbol{\nabla} \times \boldsymbol{B}_0 = \pm k_0 \boldsymbol{B}_0 = \boldsymbol{J}_0, \tag{A1}$$

where k_0 is the smallest wavenumber in the domain. The small scale component $\boldsymbol{b}'$ is composed of all the Fourier modes such that $|\boldsymbol{k}| \neq k_0$ (i.e., all the Fourier modes except the ones for which belong to B_0).

Then, the Eqs. (1) and (2) for the small scale fields become

$$\begin{aligned}\partial_t \boldsymbol{u}' = &(\boldsymbol{J}_0 \times \boldsymbol{b}') + (\boldsymbol{j}' \times \boldsymbol{B}_0) + (\boldsymbol{j}' \times \boldsymbol{b}') + \nu \boldsymbol{\Delta} \boldsymbol{u}' \\ &+ (\boldsymbol{u}' \times \boldsymbol{\omega}') - \boldsymbol{\nabla} P\end{aligned} \tag{A2}$$

and

$$\partial_t \boldsymbol{b}' = \boldsymbol{\nabla} \times (\boldsymbol{u}' \times \boldsymbol{b}') + \boldsymbol{\nabla} \times (\boldsymbol{u}' \times \boldsymbol{B}_0) - \mu \boldsymbol{\nabla} \times \boldsymbol{j}'. \tag{A3}$$

To derive the equations for the averaged kinetic and magnetic energy, we multiply Eq. (A2) by $\boldsymbol{u}'$ and Eq. (A3) by $\boldsymbol{b}'$ and we integrate over the volume V to obtain

$$\frac{1}{2}\partial_t \langle |\boldsymbol{u}'|^2 \rangle = \langle \boldsymbol{u}'(\boldsymbol{J}_0 \times \boldsymbol{b}') \rangle + \langle \boldsymbol{u}'(\boldsymbol{j}' \times \boldsymbol{B}_0) \rangle + \langle \boldsymbol{u}'(\boldsymbol{j}' \times \boldsymbol{b}') \rangle + \nu \langle |\boldsymbol{\nabla} \boldsymbol{u}'|^2 \rangle \tag{A4}$$

and

$$\frac{1}{2}\partial_t \langle |\boldsymbol{b}'|^2 \rangle = \langle \boldsymbol{j}'(\boldsymbol{u}' \times \boldsymbol{b}') \rangle + \langle j'(\boldsymbol{u}' \times \boldsymbol{B}_0) \rangle - \mu \langle |\boldsymbol{j}'|^2 \rangle, \tag{A5}$$

where $\langle . \rangle \equiv \int_V \mathrm{d}^3 x$. By summing Eqs. (A4) and (A5), we obtain

$$\begin{aligned} \partial_t (\langle |\boldsymbol{u}'|^2 \rangle + \langle |\boldsymbol{b}'|^2 \rangle) &= \langle \boldsymbol{u}'(\boldsymbol{J}_0 \times \boldsymbol{b}') \rangle - \nu \langle |\boldsymbol{\nabla} \boldsymbol{u}'|^2 \rangle - \mu \langle |\boldsymbol{j}'|^2 \rangle \\ &= k_0 \langle \boldsymbol{u}'(\boldsymbol{B}_0 \times \boldsymbol{b}') \rangle - \nu \langle |\boldsymbol{\nabla} \boldsymbol{u}'|^2 \rangle - \mu \langle |\boldsymbol{j}'|^2 \rangle. \end{aligned} \tag{A6}$$

Let $\boldsymbol{a} \equiv \boldsymbol{A}_0 + \boldsymbol{a}'$ (where $\boldsymbol{\nabla} \times \boldsymbol{A}_0 = \boldsymbol{B}_0$ and $\boldsymbol{\nabla} \times \boldsymbol{a}' = \boldsymbol{b}'$), be the vector potential. Multiplying Eq. (A3) with $\boldsymbol{a}'$ and integrating over the volume V, we obtain

$$\frac{1}{2}\partial_t \langle \boldsymbol{a}' \cdot \boldsymbol{b}' \rangle = \langle \boldsymbol{b}'(\boldsymbol{u}' \times \boldsymbol{B}_0) \rangle - \mu \langle \boldsymbol{j}' \cdot \boldsymbol{b}' \rangle, \tag{A7}$$

where $\langle \boldsymbol{a}' \cdot \boldsymbol{b}' \rangle$ is the magnetic helicity of the perturbation field. Multiplying Eq. (A7) by k_0 and then subtracting from Eq. (A6) leads to

$$\frac{1}{2}\partial_t \mathcal{M} = -\nu \langle |\boldsymbol{\nabla} \boldsymbol{u}'|^2 \rangle - \mu \langle |\boldsymbol{j}'|^2 \rangle + k_0 \mu \langle \boldsymbol{j}' \cdot \boldsymbol{b}' \rangle \tag{A8}$$

where $\mathcal{M} \equiv \langle |\boldsymbol{u}'|^2 \rangle + \langle |\boldsymbol{b}'|^2 \rangle - k_0 \langle \boldsymbol{a}' \cdot \boldsymbol{b}' \rangle$. We now show that $\mathcal{M}$ is a non-negative functional as follows:

$$\mathcal{M} = \langle |\boldsymbol{u}'|^2 \rangle + \langle |\boldsymbol{b}'|^2 \rangle - k_0 \langle \boldsymbol{a}' \cdot \boldsymbol{b}' \rangle \tag{A9}$$

$$\geq \langle |\boldsymbol{b}'|^2 \rangle - k_0 \langle \boldsymbol{a}' \cdot \boldsymbol{b}' \rangle \tag{A10}$$

$$\geq \langle |\boldsymbol{b}'|^2 \rangle - k_0 \langle |\boldsymbol{b}'|^2 \rangle^{1/2} \langle |\boldsymbol{a}'|^2 \rangle^{1/2} \tag{A11}$$

$$\geq 0, \tag{A12}$$

where the last inequality comes from noting that

$$\langle |\boldsymbol{a}'|^2 \rangle = \sum_{|\boldsymbol{k}|>k_0} k^{-2} |\hat{\boldsymbol{b}}'_k|^2 \tag{A13}$$

$$\leq \sum_{|\boldsymbol{k}|>k_0} k_0^{-2} |\hat{\boldsymbol{b}}'_k|^2 \tag{A14}$$

$$= k_0^{-2} \langle |\boldsymbol{b}'|^2 \rangle. \tag{A15}$$

The equal sign holds only for $\boldsymbol{u}' = \boldsymbol{b}' = 0$. Following the same steps, we can show that

$$-\nu \langle |\boldsymbol{\nabla} \boldsymbol{u}'|^2 \rangle - \mu \langle |\boldsymbol{j}'|^2 \rangle + k_0 \langle \boldsymbol{j}' \cdot \boldsymbol{b}' \rangle \leq 0 \tag{A16}$$

with the equality again holding only when $\boldsymbol{u}' = \boldsymbol{b}' = 0$. Thus, based on Eq. (A8), the quantity $\mathcal{M}$ will always decay until the state $\boldsymbol{u}' = \boldsymbol{b}' = 0$ is reached, which is the only case for which $\partial_t \mathcal{M} = \mathcal{M} = 0$. Therefore, all perturbations to the basic state $\boldsymbol{B}_0$ will decay to zero independently of the value of $\nu, \mu > 0$.

2. Anti-turbulence theorem for magnetically helical forcing

Here, we show that if a flow is forced only by a fully helical magnetic forcing such that $\boldsymbol{f}_b = \lambda \boldsymbol{\nabla} \times \boldsymbol{f}_b$ and $\boldsymbol{f}_u = 0$, the energy dissipation will decrease to 0 at the $\mu \to 0$ limit. For this forcing,

the balance of the magnetic helicity $H_b = \frac{1}{2}\langle \boldsymbol{a} \cdot \boldsymbol{b} \rangle$ reads

$$\epsilon_H \equiv \mu \langle \boldsymbol{j} \cdot \boldsymbol{b} \rangle = \langle \boldsymbol{a} \cdot \boldsymbol{f}_b \rangle = \lambda \langle \boldsymbol{b} \cdot \boldsymbol{f}_b \rangle = \lambda\, \epsilon, \tag{A17}$$

where ϵ is the energy dissipation rate that for this forcing $\epsilon = \langle \boldsymbol{b} \cdot \boldsymbol{f}_b \rangle$. Taking the absolute value of ϵ_H and using Schwartz inequality, we have that

$$\begin{aligned} |\epsilon_H| &= \mu |\langle \boldsymbol{j} \cdot \boldsymbol{b} \rangle| \\ &\le \mu \langle |\boldsymbol{b}|^2 \rangle^{1/2} \langle |\boldsymbol{j}|^2 \rangle^{1/2} \\ &= \sqrt{\mu} \langle |\boldsymbol{b}|^2 \rangle^{1/2} \sqrt{\mu \langle |\boldsymbol{j}|^2 \rangle} \\ &\le \sqrt{\mu} \langle |\boldsymbol{b}|^2 \rangle^{1/2} \sqrt{\mu \langle |\boldsymbol{j}|^2 \rangle + \nu \langle |\boldsymbol{\omega}|^2 \rangle} \\ &= \sqrt{\mu} \langle |\boldsymbol{b}|^2 \rangle^{1/2} \sqrt{\epsilon}. \end{aligned} \tag{A18}$$

Using (A17) and (A18), we obtain

$$|\lambda| \epsilon = |\epsilon_H| \le \sqrt{\mu} \langle |\boldsymbol{b}|^2 \rangle^{1/2} \sqrt{\epsilon}, \tag{A19}$$

thus

$$\epsilon \le \mu \langle |\boldsymbol{b}|^2 \rangle \lambda^{-2}. \tag{A20}$$

This result implies that for this forcing, the system cannot dissipate energy faster than if all dissipations took place at the forcing scale λ, and thus, a laminar scaling for the energy dissipation is followed. Note that in this case, we did not have to assume that λ is the largest scale of the system.

[1] G. Boffetta and R. E. Ecke, "Two-dimensional turbulence," Annu. Rev. Fluid Mech. **44**, 427–451 (2012).
[2] A. Pouquet and P. D. Mininni, "The interplay between helicity and rotation in turbulence: Implications for scaling laws and small-scale dynamics," Philos. Trans. R. Soc., A **368**, 1635–1662 (2010).
[3] L. M. Smith and F. Waleffe, "Generation of slow large scales in forced rotating stratified turbulence," J. Fluid Mech. **451**, 145–168 (2002).
[4] R. Marino, P. D. Mininni, D. Rosenberg, and A. Pouquet, "Emergence of helicity in rotating stratified turbulence," Phys. Rev. E **87**, 033016 (2013).
[5] C. Rorai, D. Rosenberg, A. Pouquet, and P. D. Mininni, "Helicity dynamics in stratified turbulence in the absence of forcing," Phys. Rev. E **87**, 063007 (2013).
[6] W. H. Matthaeus, D. C. Montgomery, M. Wan, and S. Servidio, "A review of relaxation and structure in some turbulent plasmas: Magnetohydrodynamics and related models," J. Turbul. **13**, N37 (2012).
[7] S. Chandrasekhar and L. Woltjer, "On force-free magnetic fields," Proc. Natl. Acad. Sci. U. S. A. **44**, 285 (1958).
[8] L. Woltjer, "A theorem on force-free magnetic fields," Proc. Natl. Acad. Sci. U. S. A. **44**, 489 (1958).
[9] J. B. Taylor, "Relaxation of toroidal plasma and generation of reverse magnetic fields," Phys. Rev. Lett. **33**, 1139–1141 (1974).
[10] H. K. Moffatt, *Magnetic Field Generation in Electrically Conducting Fluids* (Cambridge University Press, 1978).
[11] E. N. Parker, *Cosmical Magnetic Fields: Their Origin and their Activity* (Oxford University Press, 1979).
[12] D. Biskamp, *Magnetohydrodynamic Turbulence* (Cambridge University Press, 2003).
[13] W. H. Matthaeus and D. Montgomery, "Selective decay hypothesis at high mechanical and magnetic Reynolds numbers," Ann. N. Y. Acad. Sci. **357**, 203–222 (1980).
[14] S. Servidio, W. H. Matthaeus, and P. Dmitruk, "Depression of nonlinearity in decaying isotropic MHD turbulence," Phys. Rev. Lett. **100**, 095005 (2008).
[15] J. B. Taylor, "Relaxation and magnetic reconnection in plasmas," Rev. Mod. Phys. **58**, 741–763 (1986).
[16] E. N. Parker, "Magnetic neutral sheets in evolving fields. II-formation of the solar corona," Astrophys. J. **264**, 642–647 (1983).
[17] J. Heyvaerts and E. R. Priest, "Coronal heating by reconnection in dc current systems. A theory based on Taylor's hypothesis," Astron. Astrophys. **137**, 63–78 (1984).
[18] J. W. Belcher and L. Davis, "Large-amplitude alfvén waves in the interplanetary medium, 2," J. Geophys. Res. **76**, 3534–3563, doi: 10.1029/JA076i016p03534 (1971).
[19] R. Bruno and V. Carbone, "The solar wind as a turbulence laboratory," Living Rev. Sol. Phys. **2**, 4 (2005).
[20] M. Dobrowolny, A. Mangeney, and P. L. Veltri, "Fully developed anisotropic hydromagnetic turbulence in interplanetary space," Phys. Rev. Lett. **45**, 144–147 (1980).
[21] A. Pouquet, M. Meneguzzi, and U. Frisch, "Growth of correlations in magnetohydrodynamic turbulence," Phys. Rev. A **33**, 4266–4276 (1986).
[22] R. Marino, L. Sorriso-Valvo, R. D'Amicis, V. Carbone, R. Bruno, and P. Veltri, "On the occurrence of the third-order scaling in high latitude solar wind," Astrophys. J. **750**, 41 (2012).
[23] S. Servidio, C. Gurgiolo, V. Carbone, and M. L. Goldstein, "Relaxation processes in solar wind turbulence," Astrophys. J., Lett. **789**, L44 e-print arXiv:1406.3934 [astro-ph.SR] (2014).

[24] T. Stribling and W. H. Matthaeus, "Relaxation processes in a loworder threedimensional magnetohydrodynamics model," Phys. Fluids B **3**, 1848–1864 (1991).
[25] S. Servidio, W. H. Matthaeus, and V. Carbone, "Ergodicity of ideal Galerkin three-dimensional magnetohydrodynamics and Hall magnetohydrodynamics models," Phys. Rev. E **78**, 046302 (2008).
[26] P. Dmitruk and W. H. Matthaeus, "Low-frequency 1/f fluctuations in hydrodynamic and magnetohydrodynamic turbulence," Phys. Rev. E **76**, 036305 (2007).
[27] P. Dmitruk and W. H. Matthaeus, "Waves and turbulence in magnetohydrodynamic direct numerical simulations," Phys. Plasmas **16**, 062304 (2009).
[28] P. Dmitruk, P. D. Mininni, A. Pouquet, S. Servidio, and W. H. Matthaeus, "Magnetic field reversals and long-time memory in conducting flows," Phys. Rev. E **90**, 043010 (2014); e-print arXiv:1409.7568 [physics.flu-dyn].
[29] D. O. Gómez, P. D. Mininni, and P. Dmitruk, "MHD simulations and astrophysical applications," Adv. Space Res. **35**, 899–907 (2005).
[30] P. D. Mininni, D. Rosenberg, R. Reddy, and A. Pouquet, "A hybrid mpiopenmp scheme for scalable parallel pseudospectral computations for fluid turbulence," Parallel Comput. **37**, 316–326 (2011).
[31] A. C. Ting, W. H. Matthaeus, and D. Montgomery, "Turbulent relaxation processes in magnetohydrodynamics," Phys. Fluids **29**, 3261–3274 (1986).
[32] J. B. Keller, "The probability of heads," Am. Math. Mon. **93**, 191–197 (1986).